Ultrahigh-Energy-Density Supercapacitors based on All-Pseudocapacitive Binary Metal Sulfide–MXene Composites

Asrar Alam[a,d,e,f,†], Keon-Woo Kim[b,†], Hangjun Jo[b], Dhirendra Sahoo [d], Se Hyun Kim[c,], Jin Kon Kim[b,*], and Sooman Lim[a,*]*

[a] Graduate School of Flexible and Printable electronics

Jeonbuk National University, 567 Baekje-daero, Deokjin-gu, Jeonju-si, Jeollabuk-do, 54896, Republic of Korea

E-mail: smlim@jbnu.ac.kr

[b]National Creative Research Initiative Center for Hybrid Nano Materials by High-level Architectural Design of Block Copolymer

Department of Chemical Engineering, Pohang University of Science and Technology (POSTECH)

Pohang, Gyungbuk 790-784, Republic of Korea

E-mail: jkkim@postech.ac.kr

[c] Division of Chemical Engineering, Konkuk University, Seoul 05029, Republic of Korea

E-mail: shkim97@kunkuk.ac.kr

[d] Wallenberg Initiative Materials Science for Sustainability (WISE)

[e] Department of Fibre and Polymer Technology, School of Engineering Sciences in Chemistry, KTH Royal Institute of Technology, Teknikringen 56, Stockholm, 10044 Sweden

[f] Mycronic AB, Nytorpsvägen 9, Täby 183 53, Sweden

[†]Theses authors contributed equally to this work

Keywords: 2D materials, MXenes, metal sulfides, energy storage systems, supercapacitors

Materials: All chemicals were purchased from Sigma-Aldrich, except activated carbon (Korea carbon black Co. Ltd), and used without further purification.

Synthesis of c-Mx: A two-step hydrothermal method involving the synthesis of FeZnOH@$Ti_3C_2T_x$ followed by sulfidation was adopted to synthesize *c*-Mx. First, $Ti_3C_2T_x$ (1 g), zinc nitrate (1 mmol), ferrous nitrate (2 mmol), urea (7.5 mmol), and ammonium fluoride (3 mmol) were added to deionized (DI) water (60 mL) and vigorously stirred, followed by ultrasonication to create a homogeneous suspension. The resulting suspension was transferred to an autoclave and heated at 120 °C for 18 h. After completion of the reaction, the autoclave was cooled to 25 °C. Subsequently, FeZnOH@$Ti_3C_2T_x$ was obtained after washing several times using DI water and ethanol, followed by drying under vacuum conditions at 60 °C for 24 h. To obtain *c*-Mx, the sulfidation of FeZnOH@$Ti_3C_2T_x$ was conducted using a hydrothermal method. The resulting FeZnOH@$Ti_3C_2T_x$ and sodium sulfide (1.44 g) were added to DI water (60 mL) and stirred vigorously. The obtained homogeneous suspension was transferred to an autoclave and heated at 120 °C for 30 min. Finally, *c*-Mx was obtained after washing several times using DI water and ethanol, followed by drying under vacuum conditions at 60 °C for 24 h.

Synthesis of a-Mx: Similar to *c*-Mx, a two-step hydrothermal method was employed. First, $Ti_3C_2T_x$ (1 g), zinc nitrate (1 mmol), magnesium nitrate (2 mmol), urea (7.5 mmol), and ammonium fluoride (3 mmol) were added to DI water (60 mL) and vigorously stirred. This was followed by ultrasonication to obtain a homogeneous suspension. The resulting suspension was transferred to an autoclave and heated at 140 °C for 18 h. After completion of the reaction, the autoclave was cooled to room temperature. Subsequently, FeZnOH@$Ti_3C_2T_x$ was obtained after washing several times using DI water and ethanol, followed by drying under vacuum conditions at 60 °C for 24 h. To obtain *a*-Mx, the sulfidation reaction of FeZnOH@$Ti_3C_2T_x$ was conducted using a hydrothermal method. The resulting FeZnOH@$Ti_3C_2T_x$ and sodium

sulfide (1.44 g) were added to DI water (60 mL) under vigorous stirring. The obtained homogeneous suspension was transferred to an autoclave and heated at 120 °C for 30 min. Finally, *c*-Mx was obtained after washing several times using DI water and ethanol, followed by drying under vacuum conditions at 60 °C for 24 h.

Device assembly: For the precise mass loading of *c*-Mx and *a*-Mx on the current collector, we utilized printing technology. To prepare the MXene composite ink, the MXene composite (85 mg), activated carbon (15 mg), and poly(vinylidene fluoride) binder (5 mg) were added to 1 mL of *N*-methly-2-pyrrolidone and then uniformly dispersed under ultrasonication. The resulting ink was printed onto a stainless-steel current collector at 3 mg/cm^2, yielding *c*-Mx and *a*-Mx electrodes. The devices were fabricated by sandwiching a 1 M KOH aqueous electrolyte-soaked separator between *c*-Mx and *a*-Mx electrodes.

Characterization: The morphology of MXene composites was characterized by field emission scanning electron microscopy (FE-SEM, S-4800, Hitachi), high-resolution transmission electron microscopy (HR-TEM, JEM-2200FS, JEOL), X-ray diffraction (XRD, D/MAX2500 VL-PC, Rigaku) using a Cu Kα radiation source (λ = 0.154178 nm), X-ray photoelectron spectroscopy (XPS, VG ESCALAB 250, Thermo Fisher Scientific) using a monochromatic Al Kα radiation source ($h\nu$ = 1486.9 eV), and Raman spectroscopy (Alpha 300R, WITEC) using He-Ne laser with an excitation wavelength of 632.8 nm. Nitrogen physisorption experiments were performed at 77 K using a Micromeritics ASAP 2010 system.

Electrochemical Measurements: Cyclic voltammetry (CV), electrochemical impedance spectroscopy (EIS), and galvanostatic charge-discharge (GCD) measurements were performed using a potentiostat (SP 150, France). A three-electrode setup was used to test the electrochemical performances of *c*-Mx, *a*-Mx, and pristine $Ti_3C_2T_x$. The prepared sample, Hg/HgO electrode, and a Pt sheet were used as the working, reference, and counter electrodes, respectively.

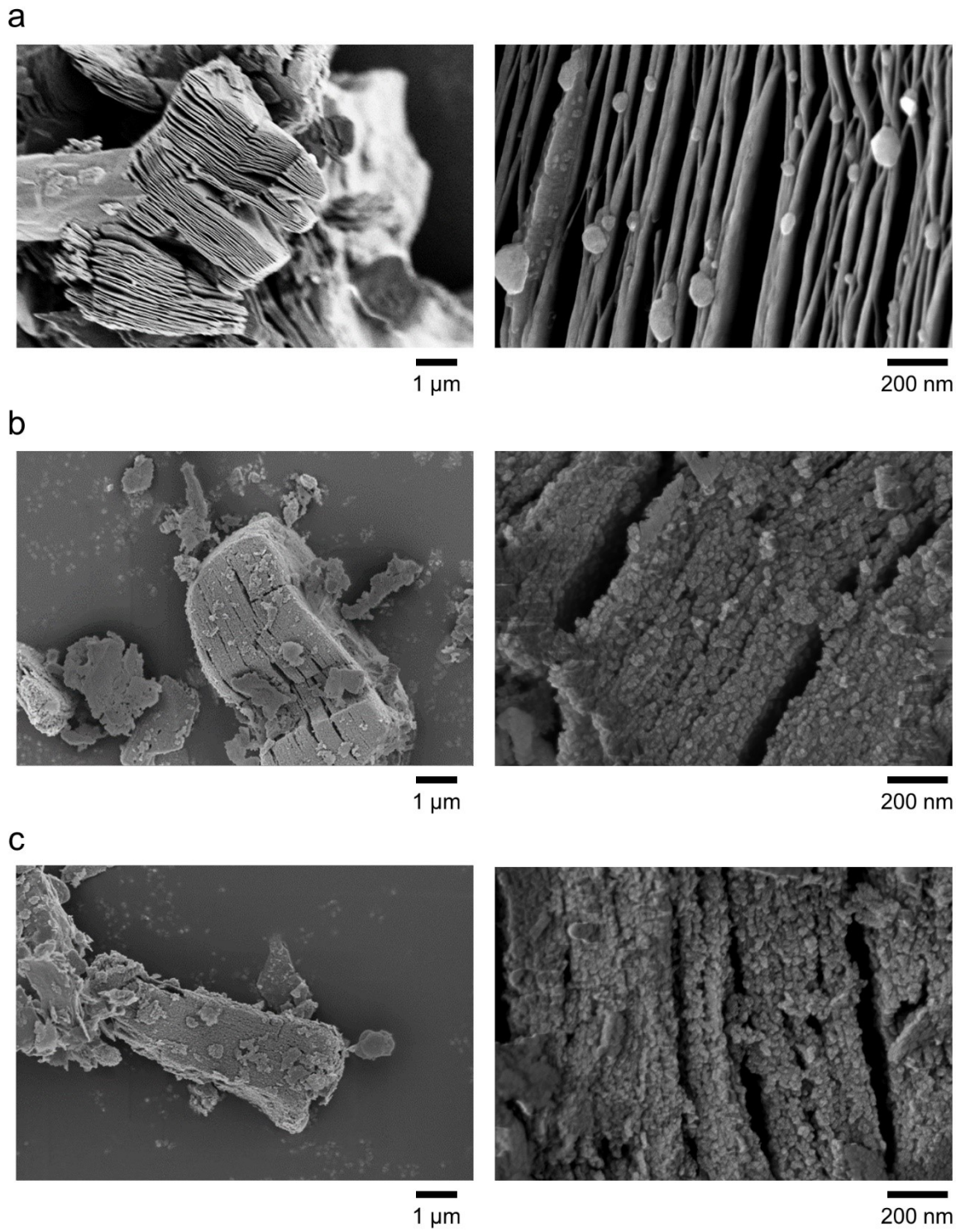

Figure S1 SEM images of (a) pristine $Ti_3C_2T_x$, (b) $Ti_3C_2T_x$@FeZnOH, and (c) $Ti_3C_2T_x$@MnZnOH. The metal hydroxide nanoparticles are uniformly decorated on the $Ti_3C_2T_x$ surface.

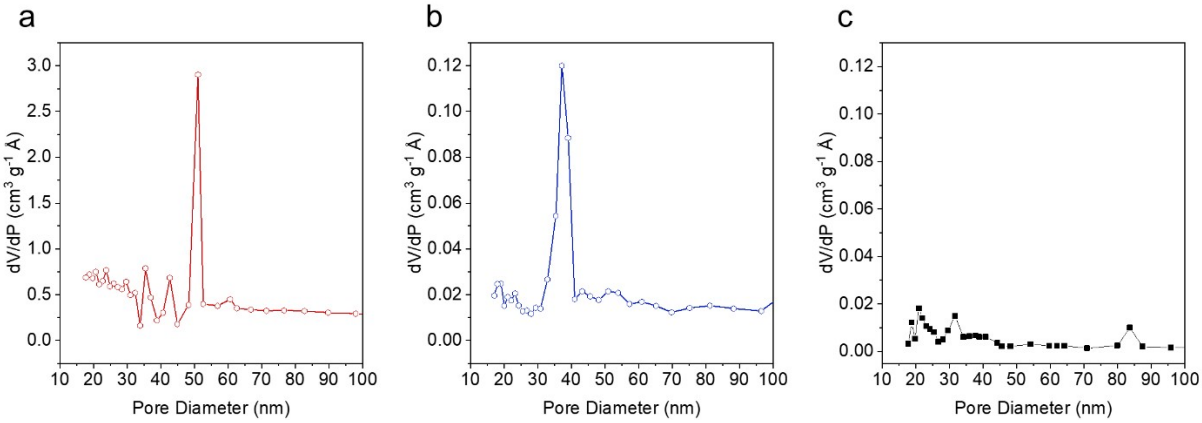

Figure S2 Pore size distribution of (a) *c*-Mx, (b) *a*-Mx, and (c) pristine $Ti_3C_2T_x$.

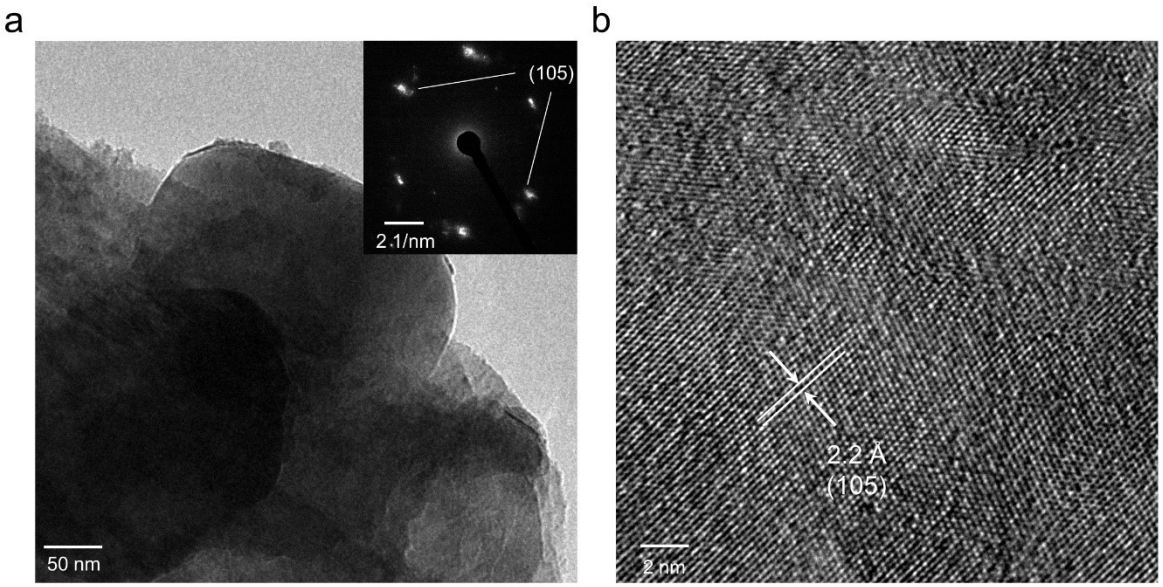

Figure S3 HR-TEM images of pristine $Ti_3C_2T_x$. (a) Low magnification (inset: SAED pattern) and (b) High magnification.

The SAED pattern with clear dot diffraction spots indicates long-range ordering of the (105) plane crystals of $Ti_3C_2T_x$. HR-TEM image further supports single crystal of $Ti_3C_2T_x$, showing lattice fringes with a *d*-spacing of 2.2 Å that correspond to the (105) lattice planes of $Ti_3C_2T_x$.

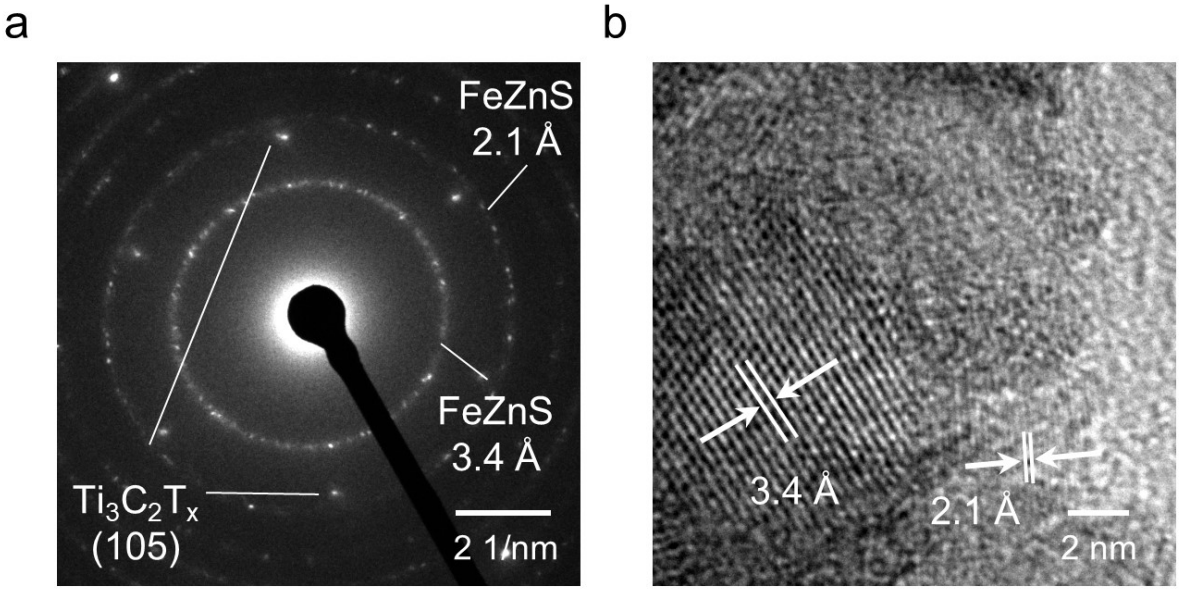

Figure S4 (a) SAED pattern of *c*-Mx and (b) HR-TEM image of FeZnS nanoparticles in *c*-Mx.

The fringe spacing of the short-range ordered nanocrystals observed in the HR-TEM image was measured to be 2.1 and 3.4 Å, which corresponds well with the concentric ring diffraction patterns of FeZnS in the SAED pattern.

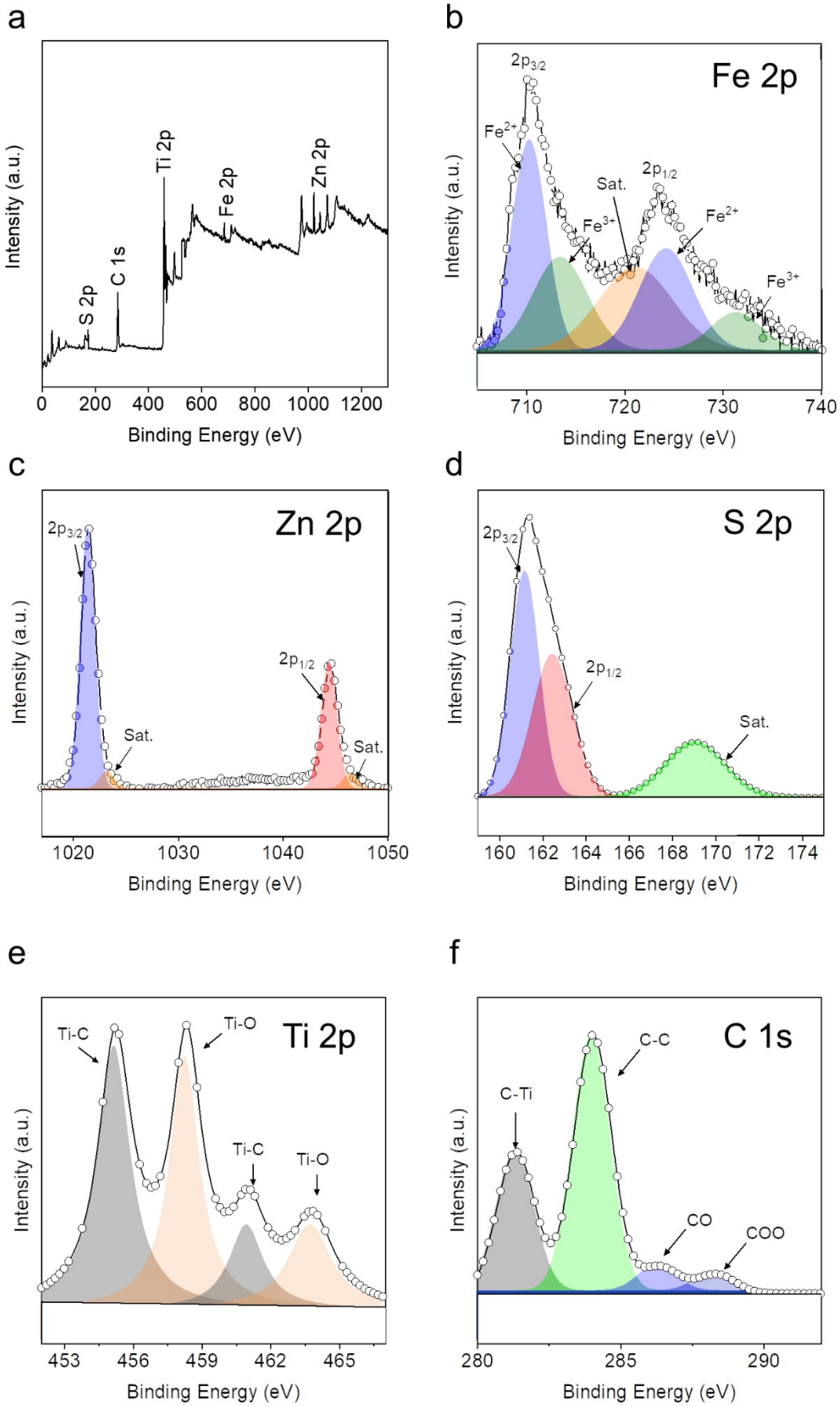

Figure S5 XPS data of *c*-Mx. (a) XPS spectra, (b) enlarged Fe 2p, (c) Zn 2p, (d) S 2p, (e) Ti 2p, and (f) C 1s.

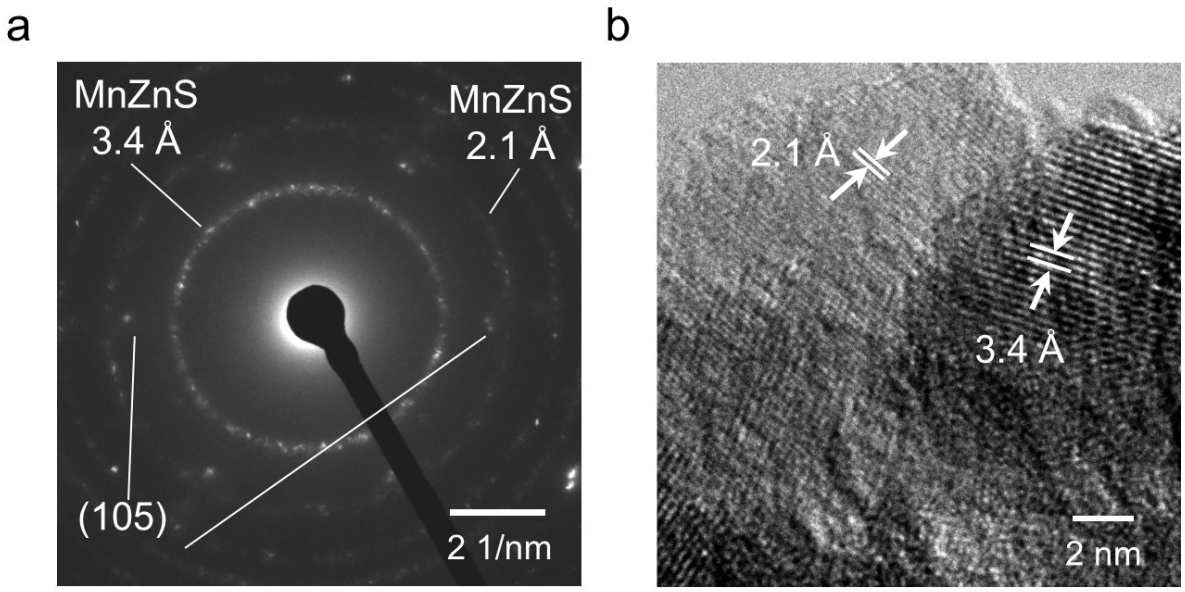

Figure S6 (a) SAED pattern of *a*-Mx and (b) HR-TEM image of MnZnS nanoparticles in *a*-Mx.

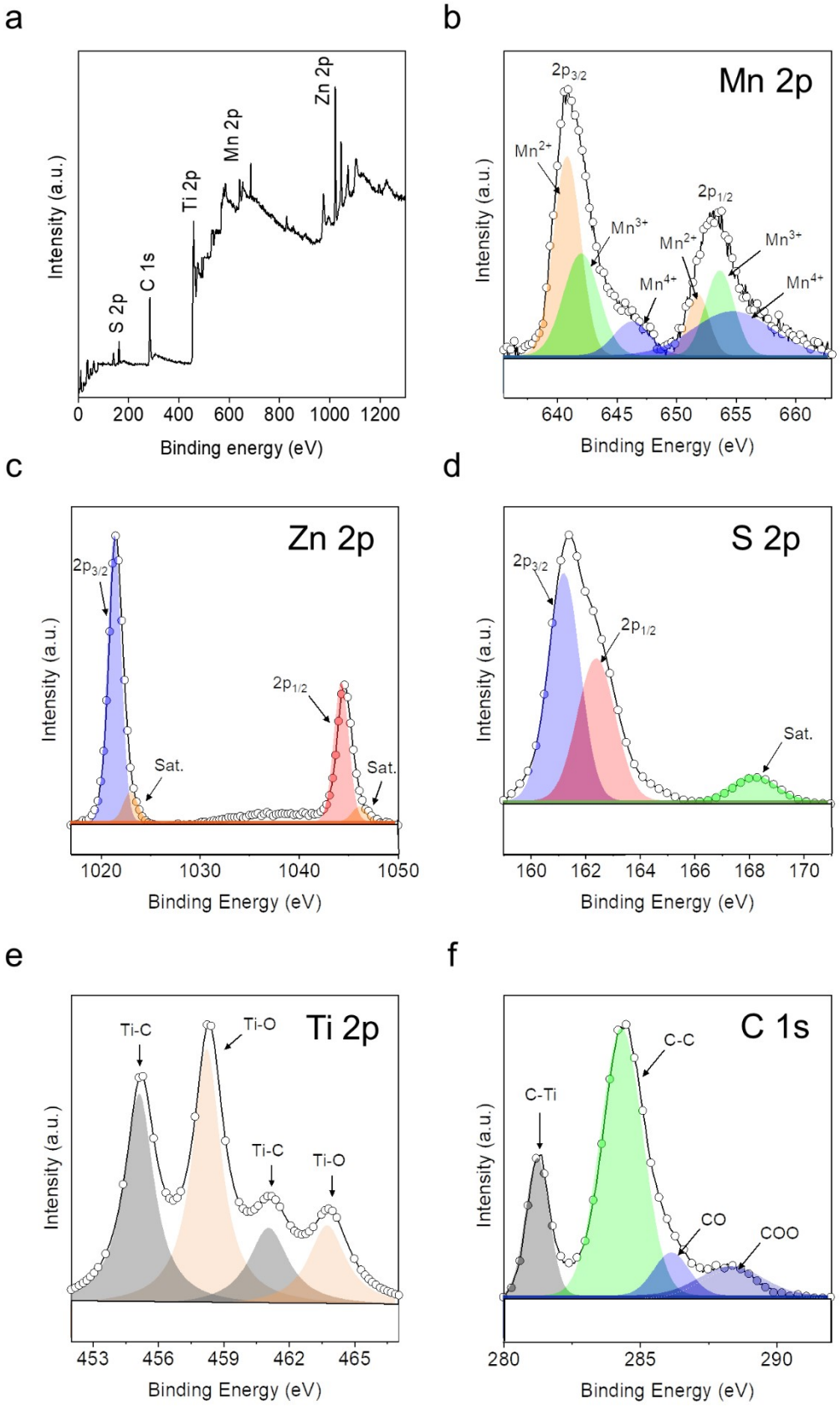

Figure S7 XPS data of *a*-Mx. (a) XPS spectra, (b) enlarged Mn 2p, (c) Zn 2p, (d) S 2p, (e) Ti 2p, and (f) C 1s.

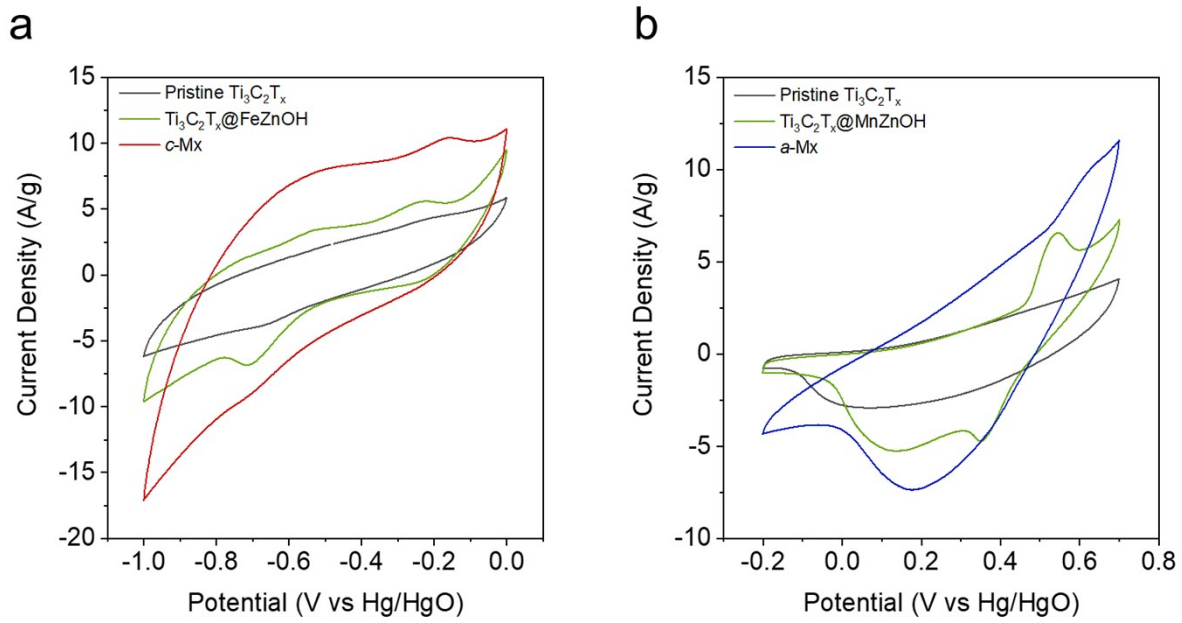

Figure S8 CV curve comparisons of (a) *c*-Mx, $Ti_3C_2T_x$@FeZnOH, and pristine $Ti_3C_2T_x$, and (b) *a*-Mx, $Ti_3C_2T_x$@MnZnOH, and pristine $Ti_3C_2T_x$.

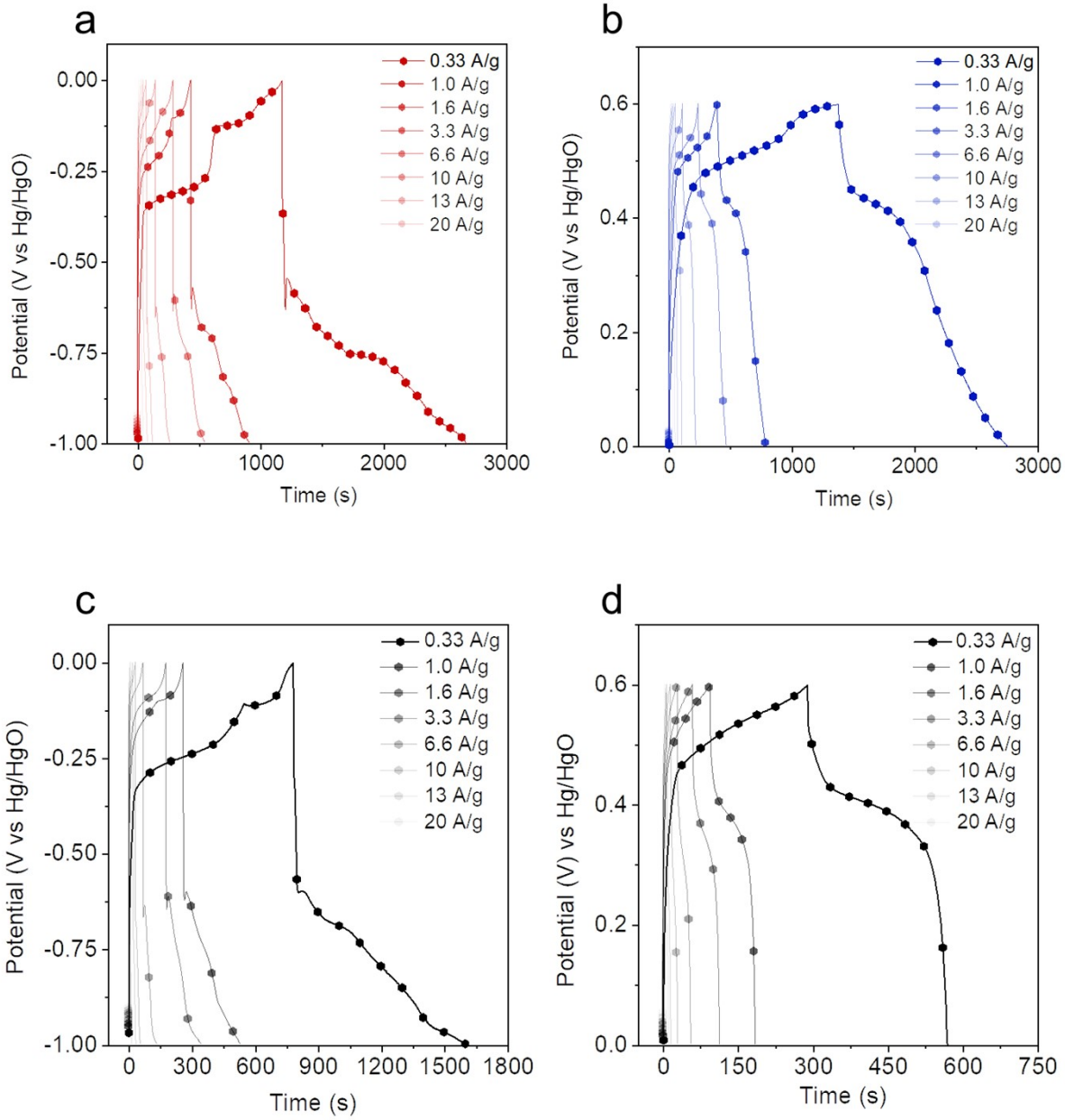

Figure S9 GCD profiles of (a) *c*-Mx, (b) *a*-Mx, and pristine $Ti_3C_2T_x$ under (c) cathodic potential and (d) anodic potential.

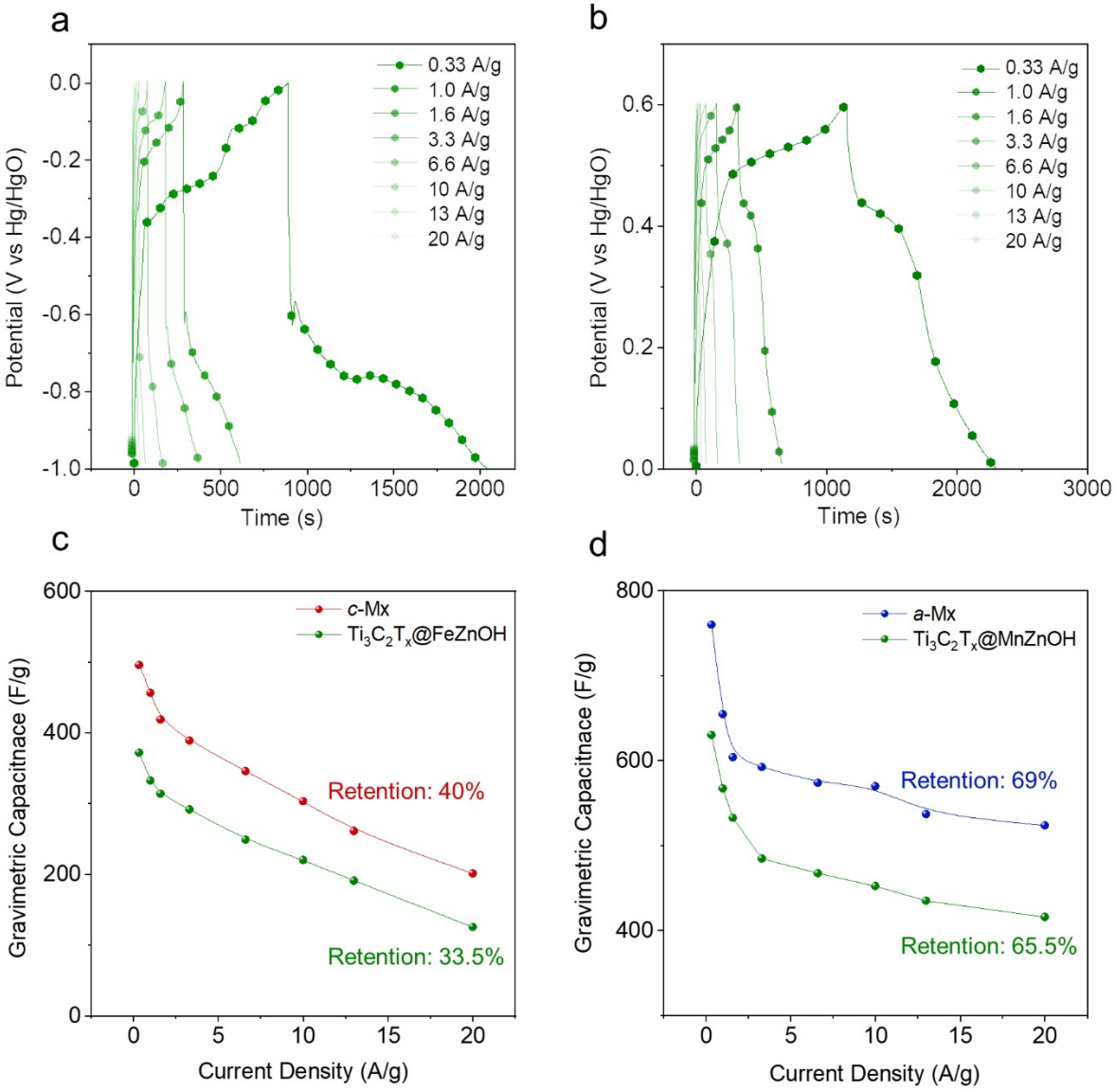

Figure S10 GCD curves of (a) $Ti_3C_2T_x$@FeZnOH and (b) $Ti_3C_2T_x$@MnZnOH. Gravimetric capacitance comparison for (c) *c*-Mx vs $Ti_3C_2T_x$@FeZnOH and (d) *a*-Mx vs $Ti_3C_2T_x$@MnZnOH.

The MXene composites showed higher energy storage performance compared to their hydroxide counterparts. For example, *c*-Mx and *a*-Mx exhibited higher gravimetric capacitance than hydroxides across all current densities. Furthermore, *c*-Mx and *a*-Mx recorded capacitance retention of 40% and 69%, respectively, surpassing those of their hydroxides, which showed 33.5% and 65.5%.

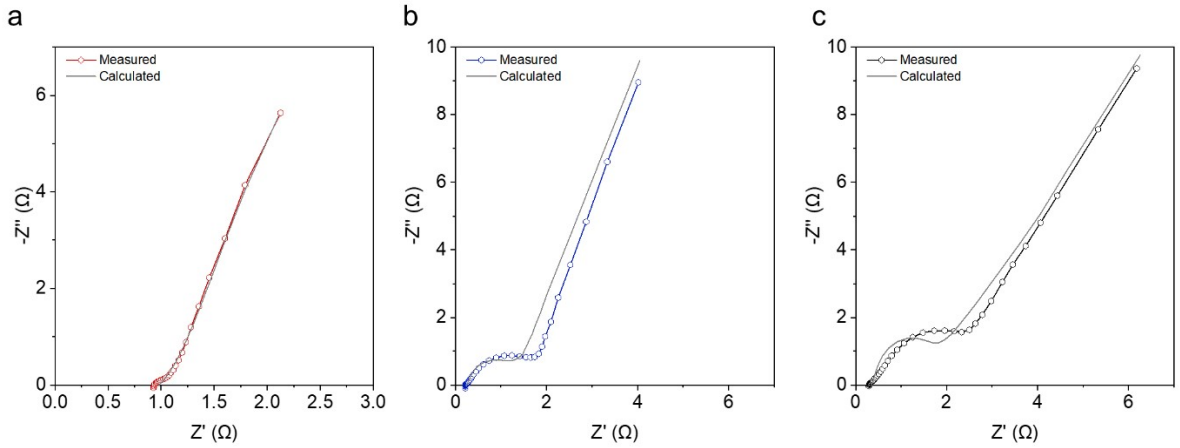

Figure S11 Measured Nyquist plots with calculated plots obtained from the equivalent circuit for: (a) *c*-Mx, (b) *a*-Mx, and (c) pristine $Ti_3C_2T_x$.

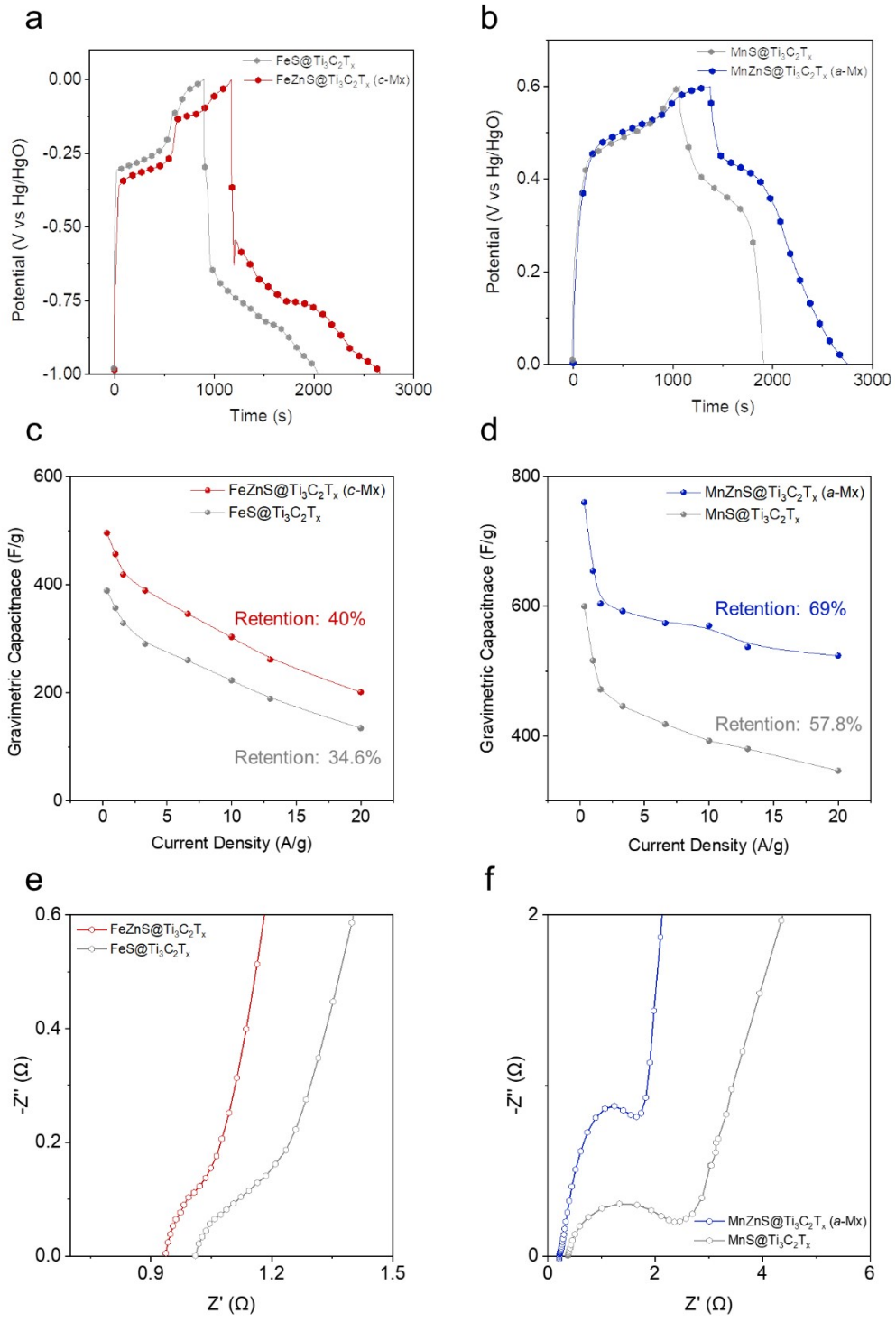

Figure S12 GCD curve comparisons of (a) *c*-Mx vs FeS@$Ti_3C_2T_x$ and (b) *a*-Mx vs MnS@$Ti_3C_2T_x$ at a current density of 0.33 A/g. Gravimetric capacitance comparison for (c) *c*-Mx vs FeS@$Ti_3C_2T_x$ and (d) *a*-Mx vs MnS@$Ti_3C_2T_x$. Nyquist plots for (e) *c*-Mx vs FeS@$Ti_3C_2T_x$ and (f) *a*-Mx vs MnS@$Ti_3C_2T_x$.

Both *c*-Mx and *a*-Mx exhibited higher gravimetric capacitance and rate performance compared to their respective $Ti_3C_2T_x$ composites with single metal sulfide nanoparticles (FeS and MnS) introduced. In Nyquist plots (Figure S12e and f), they demonstrated superior charge transport behavior at the high-frequency region, arising from the high conductivity of zinc.

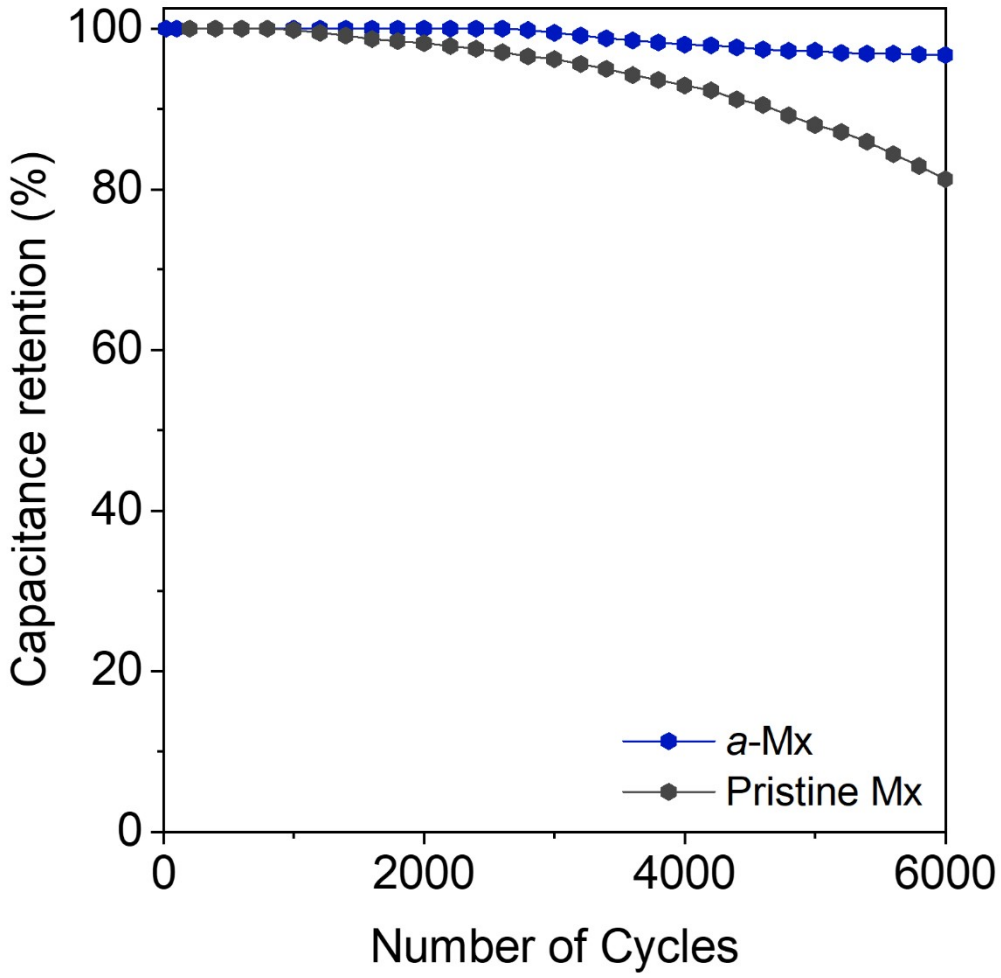

Figure S13 Cycle test of *a*-Mx and pristine $Ti_3C_2T_x$ at 20 A/g of current density.

Table S1. Comparison of electrochemical performance of the AM-SC with previously reported MXene-based SCs.

Devices	Electrolyte	Operation Voltage (V)	Energy density (Wh/kg)	Power density (W/kg)	Number of cycles (stability, %)	Ref
Graphene // Graphene@$Ti_3C_2T_x$@PANI	H_2SO_4	1.7	42.3	950	10000 (94.25)	21
$Ti_3C_2T_x$ //RuO_2	H_2SO_4	1.5	29	3800	20000 (86)	37
$Ti_3C_2T_x$@carbon // rGO@PANI	H_2SO_4	1.4	38.7	497.7	24000 (96)	38
KOH-$Ti_3C_2T_x$ // KOH-$Ti_3C_2T_x$	H_2SO_4	1.6	27.4	400	5000 (90.4)	39
$Ti_3C_2T_x$ // rGO@PANI	H_2SO_4	1.45	17	100	20000 (88.4)	40
$Ti_3C_2T_x$@MoO_3 // N-doped carbon	H_2SO_4	1.5	31.2	~300	10000 (94.2)	41
$Ti_3C_2T_x$@rGO // $Ti_3C_2T_x$@rGO	H_2SO_4	1.0	10.5	80.3	20000 (100)	42
$Ti_3C_2T_x$@rGO // $Ti_3C_2T_x$@rGO	H_2SO_4	1.0	10.8	380	10000 (100)	43
$Ti_3C_2T_x$ // rGO	H_2SO_4	1.8	34.4	1000	10000 (100)	44
$Ti_3C_2T_x$ // $Ti_3C_2T_x$@CuS	KOH	1.5	15.4	750.2	5000 (82.4)	45
rGO// $Ti_3C_2T_x$@CoS_2	KOH	1.6	28.8	800	5000 (98)	46
$Ti_3C_2T_x$ // $Ti_3C_2T_x$@NiS	KOH	1.9	20.0	500	10000 (71.4)	47
AM-SC	KOH	1.6	130.27	800.0	6000 (95)	This work